Chiral superfluid helium-3 in the quasi-two-dimensional limit: Supplemental Material

Petri J. Heikkinen,* Lev V. Levitin, Xavier Rojas, Angadjit Singh, Nathan Eng, Andrew Casey, and John Saunders
Department of Physics, Royal Holloway, University of London, Egham TW20 0EX, Surrey, United Kingdom

Anton Vorontsov
Department of Physics, Montana State University, Bozeman, Montana 59717, USA

Nikolay Zhelev,† Abhilash Thanniyil Sebastian,‡ and Jeevak M. Parpia
Department of Physics, Cornell University, Ithaca, New York 14853, USA
(Dated: March 17, 2025)

COMPARISON WITH UNSATURATED ^{3}He FILMS

In our work we investigate ^{3}He confined within a nanofabricated cavity of constant height, giving a single "film thickness", $D = 80\,\mathrm{nm}$. This height scaled by the pressure-dependent Cooper-pair size, ξ_0, as in Fig. 1c in the main text, allows comparison between different experiments, regardless of the used cavity heights.

Here we clarify the origin of the factor of two difference [45] between the "measured and effective film thicknesses" used in Ref. [44], where unsaturated (zero pressure) thin ^{3}He films of variable height grown on solid Cu disk were studied. The authors of Ref. [44] demonstrate diffuse quasiparticle scattering off the relatively rough Cu substrate and assume specular scattering off the free surface of the film. The same assumption has also been made in Refs. [47, 48, 60]. Further experimental evidence for specular scattering at a free surface is discussed in Ref. [49].

At the perfectly specular free surface the A and planar phases experience no pair breaking [60, 62]. This leads to a direct correspondence between the T_c suppression in an unsaturated thin film of thickness D on a diffusely scattering substrate and a slab of ^{3}He of thickness $2D$ confined between two diffusely scattering surfaces. The latter configuration has been theoretically considered in Ref. [63]. Good agreement with that work justified adopting $2D$ as the "effective film thickness" in Ref. [44]. When discussing the mass transport anomaly ("phase transition") reported in Ref. [44] at effective film thickness 275 nm, we halve that value to obtain the corresponding actual measured film thickness ($D \approx 137\,\mathrm{nm}$). We apply no scaling to our results. We follow Ref. [43] in using the term "effective cavity height" for the dimensionless ratio D/ξ_0, an important tuning parameter under confinement [59, 60, 63].

NEARLY SPECULAR BOUNDARY CONDITIONS

As discussed in the main manuscript, close to specular boundary conditions were achieved by preplating the silicon surfaces with a ^{4}He film of surface coverage $100\,\mu\mathrm{mol/m^2}$. Due to the preferential adsorption of ^{4}He over ^{3}He, this results in a $\sim 30\,\mu\mathrm{mol/m^2}$ solid ^{4}He layer coated with a layer of 2D superfluid ^{4}He separating liquid ^{3}He from the silicon substrate [43, 51, 52, 58]. Surface charges on silicon may affect the adsorption potential, and therefore influence the uniformity of the ^{4}He film and the specularity. To eliminate this source of disorder, we passivated the silicon substrate, thus lowering its surface charge density [70, 71]. Our approach was to chemically etch away the natural surface oxide, immediately followed by growing of a thicker than 10 nm dry thermal surface oxide layer under controlled conditions [50, 67, 72].

The influence of a ^{4}He surface boundary layer on the specularity of surface scattering of ^{3}He quasiparticles has been conducted both in the normal and superfluid states as a function of ^{4}He film thickness and ^{3}He pressure. Using torsional oscillator or transverse acoustic impedance [51–53] it has been found that approaching full specularity $S = 1$ requires a threshold finite superfluid density of the ^{4}He film. These methods are not however well-suited to detect the small departures ($S > 0.97$) from perfect specularity we are able to resolve from the T_c suppression of confined superfluid ^{3}He in the NMR experiments.

One candidate for the small decrease in specularity, present even for an ideal solid surface with perfectly uniform helium adsorption potential, is ^{3}He states within the ^{4}He film. It is well known that ^{3}He has a finite solubility in bulk ^{4}He of approximately 6%. The solubility of ^{3}He in a thin surface ^{4}He film of thickness comparable to that used here, and in contact with finite-pressure bulk (or confined) liquid ^{3}He, is not well established. It is expected to be strongly influenced by the surface: The preferential binding of ^{4}He to a surface is well understood, arising from its higher mass and hence smaller zero point energy. Thin helium mixture films have been extensively studied on heterogeneous surfaces, and more recently on the uniform binding potential surface of graphite [54, 55], which exhibit atomically layered growth. Even though theory indicates the possibility of finite density of ^{3}He states within the thin ^{4}He film, even for thin overlay of ^{3}He, the nature of interaction between these states and the ^{3}He quasiparticles outside the film is unknown. The possible effect on the surface specularity for ^{3}He could be quantified by a systematic study as a function of ^{4}He film thickness around $100\,\mu\mathrm{mol/m}^2$ and as a function of pressure. Such task was beyond the scope of this work.

Additionally, in the strongly 2D limit of a ^{3}He film, a new treatment will be required for the influence of the surface on superfluidity. For the quasi-2D films so far investigated—where the normal state Fermi surface is essentially as in 3D—the treatment is in terms of the quasiclassical theory of pair breaking by surface scattering. In the 2D limit we have an ensemble of a few 2D Fermi disks, i.e., a set of possibly weakly interacting liquids, each with its own in-plane Fermi momentum. This is expected to profoundly modify the scattering interaction at the surface. Here a treatment in terms of effective surface disorder potential could be appropriate [56].

GAP SUPPRESSION BY SPECULARITY $S = 0.98$

Any non-specular boundary condition ($S < 1.0$) suppresses the energy gap close to the surfaces, resulting in the suppression of the superfluid transition temperature T_c [60, 64]. Despite the acquired spatial dependence of the gap, the NMR precession across a cavity with $D \ll \xi_\mathrm{D}$ is uniform [82]. Here $\xi_\mathrm{D} \sim 10\,\mu\mathrm{m}$ is the dipolar length [35]. Frequency shift Δf is determined by the spatially averaged value of the squared energy gap, $\langle\Delta_0^2(z)\rangle$, and Eq. (1) in the main text can be written as [43, 61]

$$\langle\Delta_0^2(z)\rangle = \frac{\mathrm{IS}_\Delta}{\mathrm{IS}_f}\left|f^2 - f_\mathrm{L}^2\right|. \tag{S1}$$

The T_c-suppression measurements presented in Fig. 1c in the main text give surface specularity close to $S = 0.98$ within our $D = 80\,\mathrm{nm}$ cavity. The corresponding suppression of the energy gap, based on the calculations using the quasiclassical weak-coupling theory [60, 65, 76] and shown in Fig. S1a, is minuscule over the full pressure and temperature span, allowing the identification of the superfluid phase within the cavity as ^{3}He-A. Additionally, this cannot explain the observed deviation of the inferred gap values (Fig. 3 in the main text and Fig. S3 here) from the weak-coupling BCS (bulk ^{3}He-A, $S = 1.0$) temperature dependence, allowing the precise determination of the strong-coupling effects particularly visible at higher pressures. For example, at 21.0 bar the calculated squared energy gap with $S = 0.98$ deviates from the squared BCS gap by less than 1% over the full temperature range, see Fig. S1b.

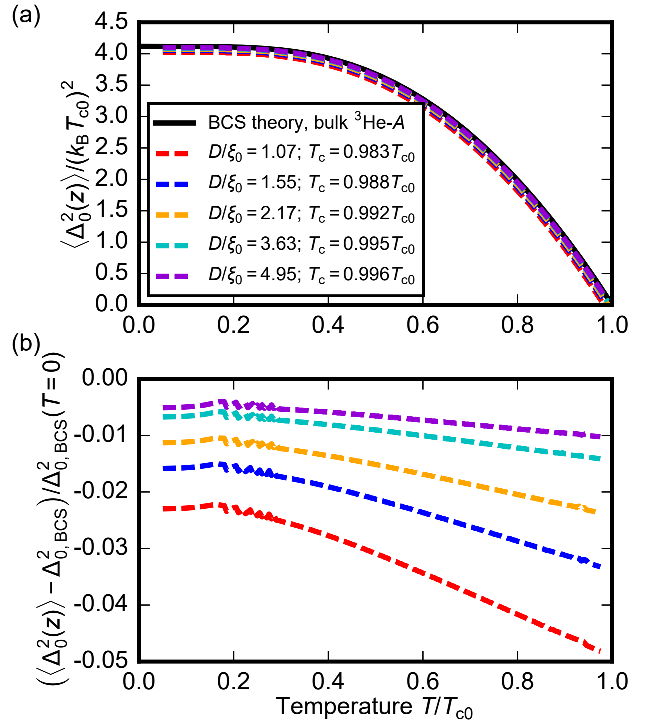

FIG. S1. (a) The spatially averaged values of the squared energy gap with specularity $S = 0.98$ corresponding to different effective cavity heights D/ξ_0 (*colored dashed lines*) do not significantly deviate from the BCS temperature dependence of the squared bulk ^{3}He-A gap, equivalent to $S = 1.0$ (*black solid line*). The quoted values of D/ξ_0 correspond to pressures 0.2, 2.5, 5.5, 12.0, and 21.0 bar within a $D = 80\,\mathrm{nm}$ high cavity, from the lowest given value of D/ξ_0 to the highest, respectively, taking into account the cavity height distortion by pressure [43]. (b) The deviation of the calculated spatially averaged values from the squared BCS gap $\Delta_{0,\mathrm{BCS}}^2$ relative to its value at $T = 0$. The relative difference smoothly decreases with decreasing temperature, with the strongest confinement (the smallest D/ξ_0) showing the largest suppression. The lines do not reach T_c0 due to small suppression of T_c, given in the legend in panel (a). The ripples visible around $T_\mathrm{c}/T_\mathrm{c0} \approx 0.2$ are artifacts of the calculations.

INITIAL SLOPES

The initial slope $\mathrm{IS}_f = \partial\left|f^2 - f_\mathrm{L}^2\right|/\partial\left(1 - T/T_\mathrm{c}\right)$ is a good indicator distinguishing between different superfluid phases. It can be determined from the linear fit for the squared precession frequency shift $\left|f^2 - f_\mathrm{L}^2\right|$ versus temperature [43, 61]. The agreement is truly linear only very close to T_c so the temperature range used in the determination of the experimental value needs to be carefully chosen. In the main text we use range $0.90T_\mathrm{c} < T < T_\mathrm{c}$ which is a suitable compromise between precision and accuracy, taking into account the number of data points within the range and the related uncertainties [43]. Initial slope defined this way

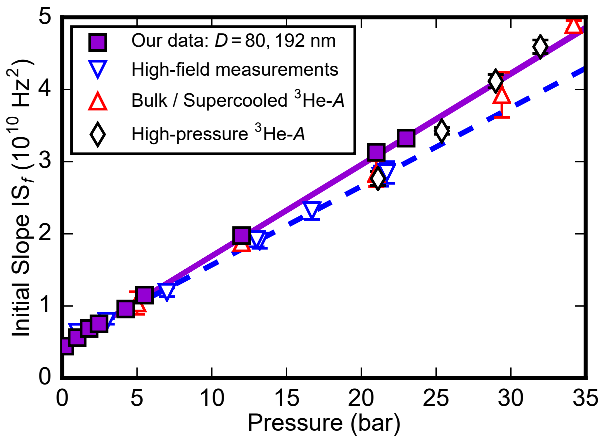

FIG. S2. Initial slopes of frequency shift versus temperature determined within range $0.95T_c < T < T_c$ compared to previous bulk ^{3}He-A experiments. *Violet squares* show the combined specular data from cavities with $D = 80\,\mathrm{nm}$ and $D = 192\,\mathrm{nm}$ [43]. *Violet line* is a linear fit to these data. The high-field experiments (*blue downward-pointing triangles*) and the linear fit (*the blue dashed line*) of the bulk ^{3}He-A initial slope are from Refs. [77–79] using the same 5% range below T_c for determining them. The data based on stable and/or supercooled bulk ^{3}He-A are from Ref. [80] (*red upward-pointing triangles*) and from Ref. [81] (*black diamonds*). In these works the used range differed from 5%, so the values have been adjusted to compensate for the systematic differences [43].

is thus ideal for the conversion between the measured frequency shift and the energy gap. However, various temperature ranges have been used to infer the values of the initial slope reported in the literature. To avoid the systematic differences and to allow comparison, we adjust the values using the relative range dependence of the initial slope of the calculated weak-coupling energy gap $\mathrm{IS}_\Delta^{\mathrm{BCS}} = \partial\Delta^2_{0,\mathrm{BCS}}/\partial(1 - T/T_{c0})$, as described in Ref. [43]. In Fig. S2 we show the data using range $0.95T_c < T < T_c$ to allow unadjusted comparison to the most complete data set from the earlier bulk ^{3}He-A experiments in Refs. [77–79]. We also combine the data measured with cavities of $D = 80\,\mathrm{nm}$ (this work) and $D = 192\,\mathrm{nm}$ [43] (data only available below $P \leq 5.5\,\mathrm{bar}$) having similar ^{4}He preplating. The other included experiments used different ranges [80, 81], so we have used the abovementioned scaling to bring those values into the same 5% range below T_c. The value of IS_f increases linearly with pressure, as seen before, and our measurements are in a good agreement with the earlier work.

TEMPERATURE DEPENDENCE OF STRONG-COUPLING EFFECTS

Near the superfluid transition temperature T_{c0} the energy gap can be described by Ginzburg-Landau (G-L) theory and directly related to the specific-heat jump ΔC_{A} at the transition. In the A phase the maximum Δ_0 of the gap in momentum space is given by [35]

$$\Delta_0^2(T) = \frac{\alpha(T)}{4\beta_{245}} = \frac{\Delta C_{\mathrm{A}}}{C_{\mathrm{N}}}(\pi k_{\mathrm{B}} T_{c0})^2(1 - T/T_{c0}), \quad \text{(S2)}$$

where $\alpha(T)$ and β_{245} are coefficients of the G-L theory. The full temperature dependence of the gap is well-established within the weak-coupling BCS theory. In this limit the scale of the gap, $\Delta_{0,\mathrm{BCS}}(T)$, is fully determined by the value of T_{c0}. However, since the experimentally observed $\Delta C_{\mathrm{A}} \propto \beta_{245}^{-1}$ is larger than the BCS value [84], the gap is enhanced by the strong-coupling effects, the more the higher the pressure.

A simple way to take this into account, used in Ref. [43], is to scale $\Delta_{0,\mathrm{BCS}}(T)$ using the established behavior near T_{c0}:

$$\Delta_0^2(T) = \frac{\Delta C_{\mathrm{A}}}{\Delta C_{\mathrm{A}}^{\mathrm{BCS}}}\Delta^2_{0,\mathrm{BCS}}(T) = \frac{\beta_{245}^{\mathrm{BCS}}}{\beta_{245}}\Delta^2_{0,\mathrm{BCS}}(T). \quad \text{(S3)}$$

Eq. (S3) successfully describes the pressure-dependence of the straight-line behavior of $\Delta_0^2(T)$ in the G-L regime, Eq. (S2), but overshoots the data at lower temperatures, see Fig. S3 and Fig. 3 in the main text. This is a manifestation of the reduction of the strong coupling effects on cooling. Wiman and Sauls have suggested to incorporate this phenomenon into the G-L theory by giving all β_i coefficients a temperature dependence [85]

$$\begin{aligned}\delta\beta_i(T) \equiv \beta_i(T) - \beta_i^{\mathrm{BCS}} &= \left(\beta_i(T_{c0}) - \beta_i^{\mathrm{BCS}}\right)\frac{T}{T_{c0}} \\ &= \delta\beta_i(T_{c0})\frac{T}{T_{c0}}, \end{aligned} \quad \text{(S4)}$$

where $\beta_i(T_{c0}) \equiv \beta_i$ is the conventional G-L parameter at T_{c0} based on a set of experiments [84]. In particular,

$$\frac{\delta\beta_{245}(T_{c0})}{\beta_{245}^{\mathrm{BCS}}} = \frac{\Delta C_{\mathrm{A}}^{\mathrm{BCS}}}{\Delta C_{\mathrm{A}}} - 1. \quad \text{(S5)}$$

Next we combine Eqs. (S3) and (S4):

$$\begin{aligned}\Delta_0^2(T) &= \frac{\beta_{245}^{\mathrm{BCS}}}{\beta_{245}(T)}\Delta^2_{0,\mathrm{BCS}}(T) \\ &= \frac{\Delta^2_{0,\mathrm{BCS}}(T)}{1 + \dfrac{\delta\beta_{245}(T_{c0})}{\beta_{245}^{\mathrm{BCS}}}\dfrac{T}{T_{c0}}}. \end{aligned} \quad \text{(S6)}$$

This model improves the agreement with the NMR data down to $T \sim 0.7T_{c0}$, consistent with the key success of Eq. (S4) in capturing the bulk A-B phase boundary $T_{\mathrm{AB}}(P)$ [85], which occurs above $\min(T_{\mathrm{AB}}) = 0.78T_{c0}$. At lower temperatures Eq. (S6) underestimates the gap, with unphysical prediction that at any pressure the weak coupling limit is reached at $T \to 0$, see Fig. S3.

A very good agreement with the experimental data is obtained by replacing T/T_{c0} in Eq. (S4) with a function

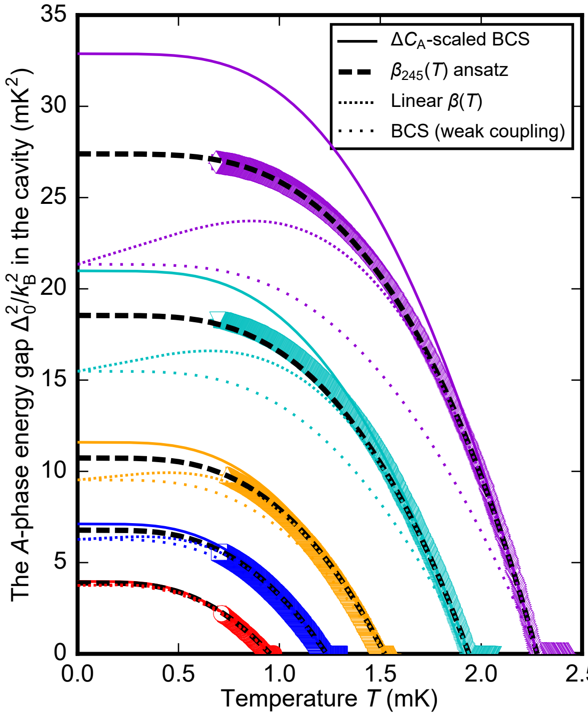

FIG. S3. Comparison of the measured and calculated energy gap. Calculations beyond the BCS T-dependence are based on Eqs. (S6) (*densely dotted lines*) and (S8) (*dashed lines*). The pressures from the lowest to the highest data set are 0.2, 2.5, 5.5, 12.0, and 21.0 bar, respectively.

of temperature behaving similarly above $0.7T_{c0}$ but not dropping all the way to zero at $T \to 0$,

$$\delta\beta_i(T) = \delta\beta_i(T_{c0})\left(1 - 0.09\frac{\Delta^2_{0,\mathrm{BCS}}(T)}{k_B^2 T_{c0}^2}\right). \tag{S7}$$

This expression, illustrated in Fig. S3 and also in Fig. 3 in the main text, leads to a successful ansatz for the temperature dependence of the energy gap:

$$\begin{aligned}\Delta_0^2(T) &= \frac{\beta_{245}^{\mathrm{BCS}}}{\beta_{245}(T)}\Delta^2_{0,\mathrm{BCS}}(T) \\ &= \frac{\Delta^2_{0,\mathrm{BCS}}(T)}{1 + \frac{\delta\beta_{245}(T_{c0})}{\beta_{245}^{\mathrm{BCS}}}\left(1 - 0.09\frac{\Delta^2_{0,\mathrm{BCS}}(T)}{k_B^2T_{c0}^2}\right)}.\end{aligned} \tag{S8}$$

Here the factor 0.09 is chosen to roughly fit the data. Since a similar expression with a freely chosen prefactor could be constructed using the B-phase gap, it remains as a task for the future to test whether Eqs. (S7) and (S8) based on the relevant weak-coupling gap values could quantitatively describe also the B phase or distorted phases under confinement.

METASTABLE PLANAR PHASE

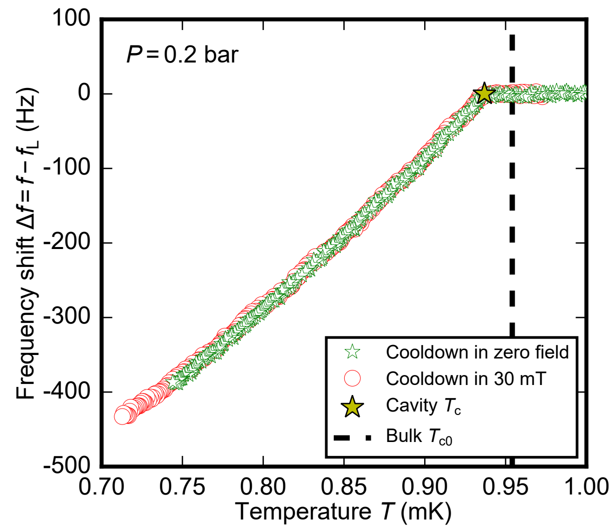

FIG. S4. The superfluid frequency shift in the $D = 80\,\mathrm{nm}$ cavity at 0.2 bar during a temperature sweep up after first cooling down through T_c with the NMR field off (*green stars*) vs. the usual NMR field on at $H_0 \approx 30\,\mathrm{mT}$ (*red circles*). Since in both cases Δf is negative and identical, the planar phase is ruled out as a possibility. Superfluid transition temperature T_c in the cavity is indicated by the *yellow star* and T_{c0} in the bulk marker by the *black dashed line*.

The A-phase order parameter in our experimental configuration ($\hat{\mathbf{d}} \perp \hat{\mathbf{z}}$ and $\hat{\mathbf{l}} \parallel \hat{\mathbf{z}}$) is written as [61]

$$\boldsymbol{\Delta}(\hat{\mathbf{p}}) = \Delta_0\,(\hat{p}_x + i\hat{p}_y)\,[|\uparrow\uparrow\rangle + |\downarrow\downarrow\rangle]\,. \tag{S9}$$

This form corresponds to $\hat{\mathbf{l}} = +\hat{\mathbf{z}}$ and is degenerate with order parameter of the form $\hat{p}_x - i\hat{p}_y$ corresponding to $\hat{\mathbf{l}} = -\hat{\mathbf{z}}$. The time-reversal invariant planar phase, which has not been observed experimentally, is degenerate with the A phase in the weak-coupling limit. Its order parameter is

$$\boldsymbol{\Delta}(\hat{\mathbf{p}}) = \Delta_0'\,(-\hat{p}_x + i\hat{p}_y)\,|\uparrow\uparrow\rangle + \Delta_0'\,(\hat{p}_x + i\hat{p}_y)\,|\downarrow\downarrow\rangle\,. \tag{S10}$$

In the weak-coupling limit these two phases have an identical energy gap, $\Delta_0 = \Delta_0'$.

In its minimum-energy state P_+, the planar phase would have a positive frequency shift. However, just like the B phase, the planar phase (which is the extreme limit of the B phase with planar distortion) can exist in a metastable dipole-energy state P_- supported by the confinement and magnetic field [61, 82, 83]. This state would have identical NMR signatures with the dipole-unlocked A phase in the confining cavity: temperature-independent magnetization, negative frequency shift, and the same tipping-angle dependence. In the weak-coupling limit, especially relevant at low pressures, the magnitudes of the frequency shift would coincide as well, making the phase identification based on NMR signatures alone challenging.

We never observed positive frequency shift arising from the cavity, so P_+ phase is out of the question. Since in normal operation we always had the polarizing $H_0 \approx 30\,\mathrm{mT}$ NMR field on, it was possible, however unlikely, to stabilize the P_- phase within the cavity each time we cooled down into the superfluid state. Such a metastable phase could not exist without a magnetic field and instead converts to P_+ at fields below the dipole field $H_\mathrm{D} \sim 3\,\mathrm{mT}$ [82]. Thus, we ruled the P_- state out by cooling through T_c in zero field at $P = 0.2\,\mathrm{bar}$. After reaching $T \approx 0.75\,\mathrm{mK}$, we ramped the field slowly back up before starting to record the NMR signals and to sweep the temperature up to characterize the superfluid frequency shift. Positive frequency shift at this point would have indicated an existence of a stable planar phase P_+. However, since Δf remained unchanged compared to the usual cooldowns (see Fig. S4), we confirmed that the dipole-unlocked A phase was stable even here.

A-PHASE GAP SIZE QUANTIZATION

In very thin superfluid films the size quantization in the momentum space results in the Fermi sphere transitioning into a series of Fermi disks, see illustration in Fig. 4 in the main text. In such a state only the energy gap values corresponding to the allowed momentum values are present, giving a possibility to avoid, e.g., any gap nodes existing in the full bulk energy gap. In the derivation below we do not consider any possible modifications to the pairing interactions by strong confinement.

The bulk A-phase energy gap is $\Delta_\mathrm{A} = \Delta_0|\sin\theta|$ where θ is the angle in momentum space between the anisotropy axis $\hat{\mathbf{l}}$ and $\hat{\mathbf{p}}$ [35]. Assuming for simplicity that the superfluid film in z-direction is trapped within an infinite potential well of width D, we get the set of allowed substates $k_z(n) = \pi n/D$ where n is an integer. If we take n_0 to be the total number of Fermi disks for $0 < k_z \leq k_\mathrm{F}$ and assume that the substate corresponding to n_0 crosses the pole, where $\theta = 0$ and $\Delta_\mathrm{A} = 0$, we have $k_z(n_0) = k_\mathrm{F}$ and $n_0 = k_\mathrm{F}D/\pi$. The value of k at the Fermi surface is $k_\mathrm{F} = 7.9\,\mathrm{nm}^{-1}$ at 0 bar and $8.9\,\mathrm{nm}^{-1}$ at 34 bar.

We can write anywhere on the Fermi sphere (we assume $0 \leq \theta \leq \pi/2$, the rest follows from the symmetry)

$$\cos\theta = \frac{k_z}{k_\mathrm{F}} \Rightarrow \sin\theta = \sqrt{1 - \frac{k_z^2}{k_\mathrm{F}^2}}. \tag{S11}$$

This allows us to write the A-phase energy gap as a function of n:

$$\Delta_\mathrm{A}(n) = \Delta_0 \sin\theta = \Delta_0\sqrt{1 - \frac{n^2}{n_0^2}}. \tag{S12}$$

If one fine tunes the above system, e.g., by adjusting P and/or D, to push the allowed values of k_z up, thus making n_0 non-integer, the nodes in the gap and the related low-energy states for the quasiparticles disappear [5]. As a result, the energy gap corresponding to the highest substate $n < n_0$ becomes the smallest allowed gap value, $\min(\Delta_\mathrm{A})$.

The larger $\min(\Delta_\mathrm{A})$ is the easier it is to cool the system down to temperatures where the gaplessness of chiral ^{3}He-A is fully manifested and the physics of two-dimensional film can be accessed [34]. For example, taking $D = 10\,\mathrm{nm}$ and $P = 0\,\mathrm{bar}$, we would have $n_0 \approx 25$ and $\min(\Delta_\mathrm{A}) \approx 0.28\Delta_0$. The corresponding temperatures in ^{3}He are accessible. The extreme confinement required to observe this effect may also suppress the superfluidity if the specularity is insufficiently close to 1. We argue that this is not the case for the boundary conditions achieved in this experiment: extrapolating the quasiclassical calculation deep into the quasi-2D regime, the $S > 0.97$ boundary condition created here will at most result in 25% suppression of T_c in a $D = 10\,\mathrm{nm}$ cavity.

---

* petri.heikkinen@rhul.ac.uk
† Current address: Department of Physics, University of Oregon, Eugene, Oregon 97403, USA
‡ Current address: VTT Technical Research Centre of Finland Ltd, Espoo 02150, Finland

[1] C. Kallin and J. Berlinsky, Chiral superconductors, Reports on Progress in Physics **79**, 054502 (2016).
[2] G. E. Volovik, Quantum Hall state and chiral edge state in thin ^{3}He-A film, JETP Letters **55**, 368 (1992).
[3] T. Kita, Angular momentum of anisotropic superfluids at finite temperatures, Journal of the Physical Society of Japan **67**, 216 (1998).
[4] M. Stone and R. Roy, Edge modes, edge currents, and gauge invariance in $p_x + ip_y$ superfluids and superconductors, Physical Review B **69**, 184511 (2004).
[5] G. E. Volovik, An analog of the quantum Hall effect in a superfluid ^{3}He film, Sov. Phys. JETP **67**, 1804 (1988).
[6] N. Read and D. Green, Paired states of fermions in two dimensions with breaking of parity and time-reversal symmetries and the fractional quantum Hall effect, Physical Review B **61**, 10267 (2000).
[7] G. E. Volovik and V. P. Mineev, Line and point singularities in superfluid ^{3}He, JETP Letters **24**, 561 (1976).
[8] M. M. Salomaa and G. E. Volovik, Half-quantum vortices in superfluid ^{3}He-A, Physical Review Letters **55**, 1184 (1985).
[9] G. E. Volovik, Monopole, half-quantum vortex, and nexus in chiral superfluids and superconductors, JETP Letters **70**, 792 (1999).
[10] D. A. Ivanov, Non-Abelian statistics of half-quantum vortices in p-wave superconductors, Physical Review Letters **86**, 268 (2001).
[11] J. A. Sauls, Surface states, edge currents, and the angular momentum of chiral p-wave superfluids, Physical Review B **84**, 214509 (2011).
[12] G. Moore and N. Read, Nonabelions in the fractional quantum Hall effect, Nuclear Physics B **360**, 362 (1991).
[13] G. E. Volovik, Fermion zero modes on vortices in chiral superconductors, JETP Letters **70**, 609 (1999).
[14] A. P. Schnyder, S. Ryu, A. Furusaki, and A. W. W. Ludwig, Classification of topological insulators and superconductors in three spatial dimensions, Physical Review B **78**, 195125 (2008).
[15] M. Sato and Y. Ando, Topological superconductors: A review, Reports on Progress in Physics **80**, 076501 (2017).
[16] A. Yu. Kitaev, Fault-tolerant quantum computation by anyons, Annals of Physics **303**, 2 (2003).
[17] C. W. J. Beenakker, Search for Majorana fermions in superconductors, Annu. Rev. Condens. Matter Phys. **4**, 113 (2013).
[18] S. Das Sarma, M. Freedman, and C. Nayak, Majorana zero modes and topological quantum computation, npj Quantum Information **1**, 15001 (2015).
[19] B. Lian, X.-Q. Sun, A. Vaezi, X.-L. Qi, and S.-C. Zhang, Topological quantum computation based on chiral Majorana fermions, Proceedings of the National Academy of Sciences **115**, 10938 (2018).
[20] S. K. Ghosh, M. Smidman, T. Shang, J. F. Annett, A. D. Hillier, J. Quintanilla, and H. Yuan, Recent progress on superconductors with time-reversal symmetry breaking, Journal of Physics: Condensed Matter **33**, 033001 (2020).
[21] A. Ramires, Symmetry aspects of chiral superconductors, Contemporary Physics **63**, 71 (2022).
[22] A. Pustogow, Y. Luo, A. Chronister, Y.-S. Su, D. A. Sokolov, F. Jerzembeck, A. P. Mackenzie, C. W. Hicks, N. Kikugawa, S. Raghu, E. D. Bauer, and S. E. Brown, Constraints on the superconducting order parameter in Sr_2RuO_4 from oxygen-17 nuclear magnetic resonance, Nature **574**, 72 (2019).
[23] H. G. Suh, H. Menke, P. M. R. Brydon, C. Timm, A. Ramires, and D. F. Agterberg, Stabilizing even-parity chiral superconductivity in Sr_2RuO_4, Physical Review Research **2**, 032023(R) (2020).
[24] V. Grinenko, D. Das, R. Gupta, B. Zinkl, N. Kikugawa, Y. Maeno, C. W. Hicks, H.-H. Klauss, M. Sigrist, and R. Khasanov, Unsplit superconducting and time reversal symmetry breaking transitions in Sr_2RuO_4 under hydrostatic pressure and disorder, Nature Communications **12**, 3920 (2021).
[25] R. Joynt and L. Taillefer, The superconducting phases of UPt_3, Reviews of Modern Physics **74**, 235 (2002).
[26] J. D. Strand, D. J. Van Harlingen, J. B. Kycia, and W. P. Halperin, Evidence for complex superconducting order parameter symmetry in the low-temperature phase of UPt_3 from Josephson interferometry, Physical Review Letters **103**, 197002 (2009).
[27] E. R. Schemm, W. J. Gannon, C. M. Wishne, W. P. Halperin, and A. Kapitulnik, Observation of broken time-reversal symmetry in the heavy-fermion superconductor UPt_3, Science **345**, 190 (2014).
[28] K. E. Avers, W. J. Gannon, S. J. Kuhn, W. P. Halperin, J. A. Sauls, L. DeBeer-Schmitt, C. D. Dewhurst, J. Gavilano, G. Nagy, U. Gasser, and M. R. Eskildsen, Broken time-reversal symmetry in the topological superconductor UPt_3, Nature Physics **16**, 531 (2020).
[29] L. Jiao, S. Howard, S. Ran, Z. Wang, J. O. Rodriguez, M. Sigrist, Z. Wang, N. P. Butch, and V. Madhavan, Chiral superconductivity in heavy-fermion metal UTe_2, Nature **579**, 523 (2020).
[30] P. K. Biswas, S. K. Ghosh, J. Z. Zhao, D. A. Mayoh, N. D. Zhigadlo, X. Xu, C. Baines, A. D. Hillier, G. Balakrishnan, and M. R. Lees, Chiral singlet superconductivity in the weakly correlated metal $LaPt_3P$, Nature Communications **12**, 2504 (2021).
[31] P. K. Biswas, H. Luetkens, T. Neupert, T. Stürzer, C. Baines, G. Pascua, A. P. Schnyder, M. H. Fischer, J. Goryo, M. R. Lees, H. Maeter, F. Brückner, H.-H. Klauss, M. Nicklas, P. J. Baker, A. D. Hillier, M. Sigrist, A. Amato, and D. Johrendt, Evidence for superconductivity with broken time-reversal symmetry in locally noncentrosymmetric SrPtAs, Physical Review B **87**, 180503(R) (2013).
[32] M. H. Fischer, T. Neupert, C. Platt, A. P. Schnyder, W. Hanke, J. Goryo, R. Thomale, and M. Sigrist, Chiral d-wave superconductivity in SrPtAs, Physical Review B **89**, 020509(R) (2014).
[33] J. A. Mydosh, P. M. Oppeneer, and P. Riseborough, Hidden order and beyond: An experimental—theoretical overview of the multifaceted behavior of URu_2Si_2, Journal of Physics: Condensed Matter **32**, 143002 (2020).
[34] G. E. Volovik, *Exotic Properties of Superfluid Helium 3*, Series in Modern Condensed Matter Physics Vol. 1 (World Scientific, Singapore, 1992).
[35] D. Vollhardt and P. Wölfle, *The Superfluid Phases of He-*

lium 3, Dover ed. (Dover Publications, New York, 2013).
[36] G. E. Volovik, *The Universe in a Helium Droplet*, International Series of Monographs on Physics Vol. 117 (Oxford University Press, Oxford, 2003).
[37] P. M. Walmsley and A. I. Golov, Chirality of superfluid ^{3}He-A, Physical Review Letters **109**, 215301 (2012).
[38] H. Ikegami, Y. Tsutsumi, and K. Kono, Chiral symmetry breaking in superfluid ^{3}He-A, Science **341**, 59 (2013).
[39] H. Ikegami, Y. Tsutsumi, and K. Kono, Observation of intrinsic magnus force and direct detection of chirality in superfluid ^{3}He-A, Journal of the Physical Society of Japan **84**, 044602 (2015).
[40] O. Shevtsov and J. A. Sauls, Electron bubbles and Weyl fermions in chiral superfluid ^{3}He-A, Physical Review B **94**, 064511 (2016).
[41] J. Kasai, Y. Okamoto, K. Nishioka, T. Takagi, and Y. Sasaki, Chiral domain structure in superfluid ^{3}He-A studied by magnetic resonance imaging, Physical Review Letters **120**, 205301 (2018).
[42] T. Mizushima, Y. Tsutsumi, M. Sato, and K. Machida, Symmetry protected topological superfluid ^{3}He-B, Journal of Physics: Condensed Matter **27**, 113203 (2015).
[43] P. J. Heikkinen, A. Casey, L. V. Levitin, X. Rojas, A. Vorontsov, P. Sharma, N. Zhelev, J. M. Parpia, and J. Saunders, Fragility of surface states in topological superfluid ^{3}He, Nature Communications **12**, 1574 (2021).
[44] J. Xu and B. C. Crooker, Very thin films of ^{3}He: A new phase?, Physical Review Letters **65**, 3005 (1990).
[45] We note that Ref. [44] reports a potential phase transition between 273 nm and 277 nm. As discussed therein, these quoted values are twice the actual measured film thickness to map unsaturated films grown on a solid substrate to slabs sandwiched between two solid walls, taking into account the expected full specularity of the free surface. See also Ref. [46].
[46] This is a reference from the main text to this Supplemental Material.
[47] J. G. Daunt, R. F. Harris-Lowe, J. P. Harrison, A. Sachrajda, S. Steel, R. R. Turkington, and P. Zawadski, Critical temperature and critical current of thin-film superfluid ^{3}He, Journal of low temperature physics **70**, 547 (1988).
[48] M. Saitoh, H. Ikegami, and K. Kono, Onset of superfluidity in ^{3}He films, Physical Review Letters **117**, 205302 (2016).
[49] H. Ikegami and K. Kono, Review: Observation of Majorana bound states at a free surface of ^{3}He-B, Journal of Low Temperature Physics **195**, 343 (2019).
[50] B. Ilic (private communication).
[51] S. M. Tholen and J. M. Parpia, Effect of ^{4}He on the surface scattering of ^{3}He, Physical Review B **47**, 319 (1993).
[52] S. Murakawa, M. Wasai, K. Akiyama, Y. Wada, Y. Tamura, R. Nomura, and Y. Okuda, Strong suppression of the Kosterlitz-Thouless transition in a ^{4}He film under high pressure, Physical Review Letters **108**, 025302 (2012).
[53] Y. Okuda and R. Nomura, Surface Andreev bound states of superfluid ^{3}He and Majorana fermions, Journal of Physics: Condensed Matter **24**, 343201 (2012).
[54] J. Saunders, B. Cowan, and J. Nyéki, Atomically layered helium films at ultralow temperatures: Model systems for realizing quantum materials, Journal of Low Temperature Physics **201**, 615 (2020).
[55] A. Waterworth, *A SQUID NMR study of ^{3}He-^{4}He mixture films adsorbed on graphite*, Ph.D. thesis, Royal Holloway, University of London (2019).
[56] P. Sharma, A. Córcoles, R. G. Bennett, J. M. Parpia, B. Cowan, A. Casey, and J. Saunders, Quantum transport in mesoscopic ^{3}He films: Experimental study of the interference of bulk and boundary scattering, Physical Review Letters **107**, 196805 (2011).
[57] A. L. Fetter and S. Ullah, Superfluid density and critical current of ^{3}He in confined geometries, Journal of Low Temperature Physics **70**, 515 (1988).
[58] M. R. Freeman, R. S. Germain, E. V. Thuneberg, and R. C. Richardson, Size effects in thin films of superfluid ^{3}He, Physical Review Letters **60**, 596 (1988).
[59] Y. Nagato and K. Nagai, A–B transition of superfluid ^{3}He in a slab with rough surfaces, Physica B: Condensed Matter **284**, 269 (2000).
[60] A. B. Vorontsov and J. A. Sauls, Thermodynamic properties of thin films of superfluid ^{3}He-A, Physical Review B **68**, 064508 (2003).
[61] L. V. Levitin, R. G. Bennett, A. Casey, B. Cowan, J. Saunders, D. Drung, Th. Schurig, and J. M. Parpia, Phase diagram of the topological superfluid ^{3}He confined in a nanoscale slab geometry, Science **340**, 841 (2013).
[62] V. Ambegaokar, P. G. deGennes, and D. Rainer, Landau-Ginsburg equations for an anisotropic superfluid, Physical Review A **9**, 2676 (1974).
[63] L. H. Kjäldman, J. Kurkijärvi, and D. Rainer, Suppression of P-wave superfluidity in long, narrow pores, Journal of Low Temperature Physics **33**, 577 (1978).
[64] Y. Nagato, M. Yamamoto, and K. Nagai, Rough surface effects on the p-wave Fermi superfluids, Journal of Low Temperature Physics **110**, 1135 (1998).
[65] A. B. Vorontsov, Andreev bound states in superconducting films and confined superfluid ^{3}He, Philosophical Transactions of the Royal Society A: Mathematical, Physical and Engineering Sciences **376**, 20150144 (2018).
[66] L. V. Levitin, R. G. Bennett, A. Casey, B. P. Cowan, C. P. Lusher, J. Saunders, D. Drung, and Th. Schurig, A nuclear magnetic resonance spectrometer for operation around 1 MHz with a sub-10-mK noise temperature, based on a two-stage dc superconducting quantum interference device sensor, Applied Physics Letters **91**, 262507 (2007).
[67] P. J. Heikkinen, N. Eng, L. V. Levitin, X. Rojas, A. Singh, S. Autti, R. P. Haley, M. Hindmarsh, D. E. Zmeev, J. M. Parpia, A. Casey, and J. Saunders, Nanofluidic platform for studying the first-order phase transitions in superfluid helium-3, Journal of Low Temperature Physics **215**, 477 (2024).
[68] S. Dimov, R. G. Bennett, A. Córcoles, L. V. Levitin, B. Ilic, S. S. Verbridge, J. Saunders, A. Casey, and J. M. Parpia, Anodically bonded submicron microfluidic chambers, Review of Scientific Instruments **81**, 013907 (2010).
[69] N. Zhelev, T. S. Abhilash, R. G. Bennett, E. N. Smith, B. Ilic, J. M. Parpia, L. V. Levitin, X. Rojas, A. Casey, and J. Saunders, Fabrication of microfluidic cavities using Si-to-glass anodic bonding, Review of Scientific Instruments **89**, 073902 (2018).
[70] R. S. Bonilla, B. Hoex, P. Hamer, and P. R. Wilshaw, Dielectric surface passivation for silicon solar cells: A review, Physica Status Solidi A **214**, 1700293 (2017).
[71] R. Kotipalli, R. Delamare, O. Poncelet, X. Tang, L. A. Francis, and D. Flandre, Passivation effects of atomic-layer-deposited aluminum oxide, EPJ Photovoltaics **4**,

45107 (2013).

[72] N. Eng, *Development of next-generation scientific platforms for moonshot quantum technologies research*, Ph.D. thesis, Royal Holloway, University of London (2024).

[73] D. S. Greywall, ^{3}He specific heat and thermometry at millikelvin temperatures, Physical Review B **33**, 7520 (1986).

[74] M. R. Freeman and R. C. Richardson, Size effects in superfluid ^{3}He films, Physical Review B **41**, 11011 (1990).

[75] S. M. Tholen and J. M. Parpia, Slip and the effect of ^{4}He at the ^{3}He-silicon interface, Physical Review Letters **67**, 334 (1991).

[76] J. W. Serene and D. Rainer, The quasiclassical approach to superfluid ^{3}He, Physics Reports **101**, 221 (1983).

[77] M. R. Rand, *Nonlinear spin dynamics and magnetic field distortion of the superfluid* ^{3}*He-B order parameter*, Ph.D. thesis, Northwestern University (1996).

[78] M. R. Rand, H. H. Hensley, J. B. Kycia, T. M. Haard, Y. Lee, P. J. Hamot, and W. P. Halperin, New NMR evidence: Can an axi-planar superfluid ^{3}He-A order parameter be ruled out?, Physica B **194-196**, 805 (1994).

[79] A. M. Zimmerman, M. D. Nguyen, and W. P. Halperin, NMR frequency shifts and phase identification in superfluid ^{3}He, Journal of Low Temperature Physics **195**, 358 (2019).

[80] P. Schiffer, M. T. O'Keefe, H. Fukuyama, and D. D. Osheroff, Low-temperature studies of the NMR frequency shift in superfluid ^{3}He-A, Physical review letters **69**, 3096 (1992).

[81] A. I. Ahonen, M. Krusius, and M. A. Paalanen, NMR experiments on the superfluid phases of ^{3}He in restricted geometries, Journal of Low Temperature Physics **25**, 421 (1976).

[82] L. V. Levitin, R. G. Bennett, E. V. Surovtsev, J. M. Parpia, B. Cowan, A. J. Casey, and J. Saunders, Surface-induced order parameter distortion in superfluid ^{3}He-B measured by nonlinear NMR, Physical Review Letters **111**, 235304 (2013).

[83] L. V. Levitin, B. Yager, L. Sumner, B. Cowan, A. J. Casey, J. Saunders, N. Zhelev, R. G. Bennett, and J. M. Parpia, Evidence for a spatially modulated superfluid phase of ^{3}He under confinement, Physical Review Letters **122**, 085301 (2019).

[84] H. Choi, J. P. Davis, J. Pollanen, T. M. Haard, and W. P. Halperin, Strong coupling corrections to the Ginzburg-Landau theory of superfluid ^{3}He, Physical Review B **75**, 174503 (2007).

[85] J. J. Wiman and J. A. Sauls, Superfluid phases of ^{3}He in nanoscale channels, Physical Review B **92**, 144515 (2015).

[86] J. J. Wiman, *Quantitative superfluid helium-3 from confinement to bulk*, Ph.D. thesis, Northwestern University (2018).

[87] J. Saunders, Realizing quantum materials with helium: Helium films at ultralow temperatures, from strongly correlated atomically layered films to topological superfluidity, in *Topological Phase Transitions and New Developments*, edited by L. Brink, M. Gunn, J. V. José, J. M. Kosterlitz, and K. K. Phua (World Scientific Publishing, Singapore, 2019) pp. 165–196.

[88] H. Wu and J. A. Sauls, Weyl Fermions and broken symmetry phases of laterally confined ^{3}He films, Journal of Physics: Condensed Matter **35**, 495402 (2023).

[89] P. J. Heikkinen, L. V. Levitin, X. Rojas, A. Singh, N. Eng, A. Vorontsov, N. Zhelev, T. S. Abhilash, J. M. Parpia, A. Casey, and J. Saunders, Accompanying data for "Chiral superfluid helium-3 in the quasi-two-dimensional limit" (2024), Figshare.